1   **High-throughput functional mapping of variants in an arrhythmia gene, *KCNE1*, reveals novel**

2   **biology**

3

4   **Authors:** Ayesha Muhammad,[1,2] Maria E. Calandranis,[3] Bian Li,[3] Tao Yang,[3] Daniel J. Blackwell,[3]

5   M. Lorena Harvey,[3] Jeremy E. Smith,[3] Ashli E. Chew,[3] John A. Capra,[4] Kenneth A. Matreyek,[5]

6   Douglas M. Fowler,[6] Dan M. Roden,*[,1,3,7,8] and Andrew M. Glazer.*[,1,3]

7

8   **Affiliations:**

9   1.   Vanderbilt Genetics Institute, Vanderbilt University Medical Center, Nashville, TN

10   37232, USA.

11   2.   Medical Scientist Training Program, Vanderbilt University, Nashville, TN 37232, USA.

12   3.   Department of Medicine, Vanderbilt University Medical Center, Nashville, TN 37232,

13   USA.

14   4.   Bakar Computational Health Sciences Institute and Department of Epidemiology and

15   Biostatistics, University of California, San Francisco, CA 94143, USA.

16   5.   Department of Pathology, Case Western Reserve University School of Medicine,

17   Cleveland, OH 44106, USA.

18   6.   Department of Genome Sciences, University of Washington, Seattle, WA 98195,

19   USA.

20   7.   Department of Biomedical Informatics, Vanderbilt University Medical Center,

21   Nashville, TN 37232, USA.

22   8.   Department of Pharmacology, Vanderbilt University Medical Center, Nashville, TN

23   37232, USA.

24

25   * These authors contributed equally.

26   Correspondence: Andrew M. Glazer andrew.m.glazer@vumc.org.

33 **Abstract**

34 Background:

35 *KCNE1* encodes a 129-residue cardiac potassium channel (I_{Ks}) subunit. KCNE1 variants are

36 associated with long QT syndrome and atrial fibrillation. However, most variants have

37 insufficient evidence of clinical consequences and thus limited clinical utility.

38

39 Results:

40 Here, we demonstrate the power of variant effect mapping, which couples saturation

41 mutagenesis with high-throughput sequencing, to ascertain the function of thousands of

42 protein coding KCNE1 variants. We comprehensively assayed KCNE1 variant cell surface

43 expression (2,554/2,709 possible single amino acid variants) and function (2,539 variants). We

44 identified 470 loss-of-surface expression and 588 loss-of-function variants. Out of the 588 loss-

45 of-function variants, only 155 had low cell surface expression. The latter half of the protein is

46 dispensable for protein trafficking but essential for channel function. 22 of the 30 KCNE1

47 residues (73%) highly intolerant of variation were in predicted close contact with binding

48 partners KCNQ1 or calmodulin. Our data were highly concordant with gold standard

49 electrophysiological data (ρ = -0.65), population and patient cohorts (32/38 concordant

50 variants), and computational metrics (ρ = -0.55). Our data provide moderate-strength evidence

51 for the ACMG/AMP functional criteria for benign and pathogenic variants.

52

53 Conclusions:

54   Comprehensive variant effect maps of *KCNE1* can both provide insight into I_{Ks} channel biology

55   and help reclassify variants of uncertain significance.

56

57   Keywords:

58   KCNE1, saturation mutagenesis, multiplexed assay of variant effect, long QT syndrome, variant

59   classification

60

61

62 **Background**

63   Loss-of-function variants in *KCNE1* can cause type 5 long QT syndrome (LQT5; MIM

64 613695), a cardiac arrhythmia disorder characterized by QT prolongation on the

65 electrocardiogram and an increased risk of sudden cardiac death.[1] Heterozygous LQT5 variants

66 can cause isolated QT prolongation (also known as Romano-Ward Syndrome),[2] and

67 homozygous and compound heterozygous variants can cause both QT prolongation and

68 deafness (Jervell and Lange-Nielsen Syndrome; MIM 612347).[3] Almost 50 unique *KCNE1*

69 variants have been observed in patients with LQT5.[1,4–6] In addition, two gain-of-function

70 variants have been associated with atrial fibrillation in isolated families.[7] *KCNE1* encodes a

71 single-spanning transmembrane protein that acts as a modulatory subunit to the pore-

72 conducting KCNQ1 to form the I_{Ks} channel critical for cardiac repolarization (Figure 1A). The I_{Ks}

73 complex is conventionally thought of as comprising KCNE1 and KCNQ1. However, additional

74 proteins, including calmodulin, interact with the complex to modulate channel

75 electrophysiology.[8] *KCNE1* variants can disrupt channel function in two major ways: by reducing

76 cell surface expression or by altering gating to reduce potassium flux.[9]

77   The American College of Medical Genetics and Genomics/Association of Molecular

78 Pathology (ACMG/AMP) criteria are used to classify variants as pathogenic, likely pathogenic,

79 likely benign, or benign.[10] Variants with inconclusive evidence for clinical classification are

80 designated as variants of uncertain significance (VUS). For many Mendelian disease genes,

81 including *KCNE1*, most discovered variants are VUS and thus have limited impact on clinical

82 decision-making,[10] presenting a major challenge to genomic medicine.[11,12] In the ClinVar

83 database of variant classifications,[13] 77.4% of *KCNE1* variants are either VUS or have conflicting

84   interpretations (Figure 1B). These variants, together with those reported by gnomAD or clinical

85   case studies, represent a small subset of all possible missense variants (Figure 1C). It has been

86   proposed that all missense variants compatible with life likely already exist in ~50 individuals on

87   the planet.[14] In the ACMG/AMP scheme, well-validated *in vitro* functional studies can provide

88   up to strong-level evidence for the PS3 (damaging effect on protein) and BS3 (no damaging

89   effect) criteria.[15,16] However, functional assessment lags behind the rate of VUS discovery due

90   to the rapid increase of genetic testing in research and clinical domains.[12] One way to address

91   this VUS problem is to leverage multiplexed assays for variant effects (MAVEs) to test

92   thousands of variants in a single, highly-multiplexed experiment.[12,17] In a MAVE, a

93   comprehensive variant library is coupled to a selection assay and high-throughput sequencing

94   to ascertain variant function.

95   In this study, we conducted multiplexed assays of variant cell surface expression and

96   potassium flux on a library of 2,592 single residue KCNE1 variants (95.7% of 2,709 total possible

97   variants, Figure S1). We used an HA epitope in KCNE1 to determine cell surface expression of

98   2,554 individual variants using a "landing pad" cell line,[18] which integrates a single variant per

99   cell. This assay identified 470 missense variants that decrease and 310 that increase cell surface

100   expression. We also used a gain-of-function KCNQ1 variant to design a cell survival assay that

101   selects against cells with functioning channels. We deployed the function assay on 2,539 KCNE1

102   variants and found 588 loss-of-function missense variants, only 155 of which also had low cell

103   surface expression. These datasets correlate well with previously validated *in vitro* studies,

104   computational predictors, population metrics, and clinical phenotypes. Our data provide insight

7

105   into KCNE1 structure and biology and can be implemented to reclassify variants in the

106   ACMG/AMP scheme.

107

108   **Results**

109

110   ***Validation of an extracellular KCNE1 HA tag to detect cell surface expression***

111   We cloned a 9-residue hemagglutinin (HA) tag into the extracellular domain of *KCNE1*

112   (between residue 33 and 34; Figure 1A). KCNE1-HA (33-34) resulted in 3-fold higher cell surface

113   labeling of the I_{Ks} channel complex compared to a previously described HA tag located in a

114   predicted alpha helix (Figure S2A).[19] Neither I_{Ks} peak and tail current densities, nor

115   activation/inactivation properties were significantly different between KCNE1-WT and KCNE1-

116   HA (Figure 1D). Human Embryonic Kidney (HEK) 293T landing pad cells expressing *KCNE1*-HA

117   were labeled with a fluorophore-conjugated anti-HA antibody, visualized by confocal

118   microscopy, and quantified by flow cytometry (Figures 1E and 1F). In cells expressing *KCNE1*-HA

119   only, minimal plasma membrane anti-HA labeling was present, consistent with previous

120   studies.[9,20] In contrast, cells co-expressing both *KCNE1*-HA and *KCNQ1* demonstrated

121   substantial plasma membrane anti-HA labeling in live cells, and both plasma membrane and

122   intracellular labeling in permeabilized cells (Figure 1E).[9,21] Quantification of cell surface

123   expression by flow cytometry confirmed these observations (Figure 1F). A minimal but

124   detectable amount of plasma membrane labeling was seen in *KCNE1*-HA only cells but the

125   addition of *KCNQ1* caused a 6.1-fold increase in cell surface expression (Figures 1F and S2B). As

126   expected, a known loss-of-trafficking variant (L51H) had minimal cell surface expression and a

127   known gating variant (D76N) had near-WT cell surface expression when co-expressed with

128   *KCNQ1* (Figures 1F and S2B).[22]

129

130   **A comprehensive library of KCNE1 mutations**

131   We generated a comprehensive variant library of the 129-residue KCNE1 protein

132   associated with random 18-mer barcodes using inverse PCR mutagenesis with degenerate

133   primers (See *Methods*, Figure S3A).[23] We linked 80,282 barcodes to 2,368 missense, 100

134   synonymous, and 124 nonsense KCNE1 variants (95.7% of the total possible variants; Figure

135   S3B). Each variant was represented by a mean of 31 barcodes (Figure S3C).

136

137   **Multiplexed assay of KCNE1 cell surface expression**

138   We coupled antibody labeling of the extracellular HA tag to deep sequencing of the

139   library barcodes to perform a multiplexed assay of KCNE1 cell surface expression in cells

140   engineered to constitutively express *KCNQ1* (Figure 2A). After quality control (see *Methods*;

141   Figure S4A), we obtained cell surface trafficking scores for 98 synonymous, 117 nonsense, and

142   2,339 missense variants (94.2% of all possible variants; Figure 2B). Scores calculated from three

143   individual replicates were highly concordant (Spearman's ρ = 0.81-0.87, p < 0.001; Figure S4B).

144   Cell surface trafficking scores for synonymous variants were normally distributed (0.988-1.024,

145   95% CI, Figures 2B-C). Nonsense variant scores were bimodally distributed (mode 1 = 0.01,

146   mode 2 = 0.74). Nonsense variants from residue 1 to 55 were all trafficking-deficient, whereas

147   nonsense variants at or after residue 56 had near-WT or higher than WT cell surface expression

148   (p = 2.5×10^{-20}, Wilcoxon test; Figures 2B-C). We therefore classified nonsense variants as early

149   nonsense (residue 1-55) and late nonsense (56-129) in all subsequent trafficking analyses. All

150   variants at residue 1 were trafficking-null as expected.

151   Missense variants with score estimates (95% confidence interval) lower than 2.5th

152   percentile or higher than 97.5th percentile of the synonymous variant distribution were

153   assigned as loss- or gain-of-trafficking respectively. Using these cutoffs, we identified 470 loss-

154   of-trafficking variants and 311 gain-of-trafficking variants. We also compared trafficking scores

155   to the few literature reports of cell surface trafficking measurements, typically reported as

156   "normal" or "loss-of-trafficking." 7/9 variants were concordant: 6 variants with normal or near-

157   normal trafficking (T6F, S74L D76A, D76N, Y81C, and W87R) and 1 loss-of-trafficking variant

158   (L51H; Figure S4C).[22,24−26] Two discordant variants, R98W and G52R, were previously reported

159   to have normal trafficking but were loss-of-trafficking in our assay.[9]

160   Several interesting and previously unreported findings emerged from the cell surface

161   trafficking scores (Figure 2F). As mentioned above, nonsense variants after residue 55 were still

162   able to traffic to the cell surface. In the extracellular N-terminus, almost all cysteine variants

163   from residue 2 to 33 had increased cell surface expression. Residues 46-59 in the

164   transmembrane helix, likely juxtaposed to the hydrophobic core of the lipid bilayer, were highly

165   resistant to polar or charged variation. Variants in residues 61-70, interacting with the

166   intracellular hydrophilic edge of the cell membrane, increased cell surface expression. Predicted

167   alpha helices in the intracellular C-terminus (residues 79-114) had multiple residues resistant to

168   aromatic or larger aliphatic variation.

169   As HEK293T cells only expressing KCNE1 exhibited detectable levels of anti-HA staining,

170   we conducted a second MAVE of KCNE1 cell surface expression in the absence of co-expressed

171   KCNQ1 ("KCNQ1-"; Figure S5) to explore their intermolecular interaction. Trafficking scores for

172   missense variants in the presence and absence of *KCNQ1* were highly correlated (Figure 2D,

173   Spearman's ρ = 0.88, p < 2×10^{-6}), except for variants in the N-glycosylation sequons (NXS/NXT

174   motifs) at positions 5-7 and 26-28 in the extracellular N-terminus of KCNE1.[26,27] Most variants

175   disrupting N-glycosylation especially at residues 26 and 28 reduced cell surface expression in

176   the absence of KCNQ1 (Figure 2D). Thus, loss of N-terminal glycosylation is more advantageous

177   to cell surface expression in the presence of KCNQ1. Cell surface expression of cysteine super-

178   trafficking variants (including at the 5-7 and 26-28 glycosylation sequons) was not affected by

179   KCNQ1. As discussed below, this result may reflect antagonism between KCNE1 N-glycosylation

180   and KCNE1/KCNQx interaction unique to KCNQ1 and not other binding partners possibly

181   expressed in HEK293T cells.

182

183   ***Development of a cell fitness assay for KCNE1 function***

184   Since I_{Ks} channels are closed at the resting potential of HEK293T cells (approximately -25

185   mV),[28] we developed an assay for KCNE1 function by leveraging the electrophysiology of a

186   previously described gain-of-function variant, KCNQ1-S140G.[29,30] In the presence of KCNE1,

187   KCNQ1-S140G left-shifts the voltage of I_{Ks} channel activation[29] and reduces channel

188   deactivation;[31] in the absence of KCNE1, the channel expresses minimal current (Figure 3A).

189   These electrophysiological shifts result in substantial KCNE1-dependent K^+ efflux at -25 mV. We

190   hypothesized that long-term expression of I_{Ks} channels formed by KCNQ1-S140G and normally

191   functioning KCNE1 would decrease cell fitness due to continual K^+ efflux. To test this

192   hypothesis, we integrated a 1:1 mixture of empty vector control and either wild-type KCNE1-HA

193   or previously studied KCNE1 variants into HEK293T landing pad cells stably expressing KCNQ1-

194   S140G (LP-KCNQ1-S140G, Figure 3B). We then quantified KCNE1$^+$ and KCNE1$^-$ cell proportions

195   over 20 days (Figure 3C and 3D). Compared to cells with empty vector controls, cells with WT

196   KCNE1 depleted over time, whereas cells with loss-of-function KCNE1 variants (L51H or D76N)

197   persistently survived. Two previously described KCNE1 gain-of-function variants (G60D and

198   G25V)[7] depleted at the same rate as KCNE1-HA-WT (Figure 3D), indicating that this assay does

199   not distinguish gain-of-function variants from WT.

200

201   ***Multiplexed assay of KCNE1 function***

202   We used this KCNQ1-S140G-based cell fitness assay to conduct a multiplexed assay of

203   KCNE1 function. We integrated the KCNE1 library into HEK293T cells stably expressing KCNQ1-

204   S140G and quantified cell survival over 20 days (Figure 4A). After 20 days, cell expressing

205   synonymous variants were depleted and those expressing most nonsense variants persistently

206   survived (Figure S6A). These changes in the cell pool were not seen in the presence of WT-

207   KCNQ1 (Figure S6B). Variant depletion from day 0 to day 20 was used to calculate normalized

208   KCNE1 function scores for 98 synonymous, 121 nonsense, and 2,320 missense variants (93.7%

209   of all variants; Figures 4B and S6C). Function scores across three replicates were highly

210   concordant (Spearman's ρ=0.87; Figure S6D). Synonymous variants followed an asymmetric

211   unimodal distribution (median = 0.99, IQR=0.27, Figure 4B). Nonsense variants were bimodally

212   distributed (mode 1 = 0.02, mode 2 = 0.99); nonsense variants at residues 1-104 were loss-of-

213   function, whereas nonsense variants at residue 105-129 had WT-like function (p = 2.6x10^{-13},

214   Wilcoxon test, Figure 4C). Thus, across the trafficking and function assays, three classes of

215   nonsense variants were present based on residue number: #1-55 caused loss of trafficking and

216   function, #56-104 caused WT-like or elevated trafficking but loss-of-function, and #105-129

217   caused near WT-like trafficking and function (Figure S7A). All variants at residue 1 were loss-of-

218   function as expected. Missense variant function scores were bimodally distributed (mode 1 =

219   0.14, mode 2 = 1.04). The two modes approximately corresponded to the peaks of the

220   synonymous distribution and early nonsense distributions. Upon comparing trafficking and

221   function scores for missense variants, we found 136 trafficking-null and 288 trafficking-normal,

222   functionally deleterious variants (Figure 4D). We refer to the latter as "gating variants."

223   On the heatmap of KCNE1 function scores, variation-resistant regions were located in

224   the transmembrane helix (residues 61-73) and the transmembrane-proximal cytosolic alpha

225   helix (residues 77-82; Figure 4F). Known trafficking-null variants (L51H) and gating variants

226   (D76N, W87R) had deleterious function scores.[22] Common polymorphisms (G38S, D85N) had

227   WT-like trafficking and function scores, consistent with their minimal effects on baseline QT

228   interval. Residue 85 is otherwise resistant to variation and D85N is only one of 2 missense

229   variants at this residue with WT-like score estimates (D85N: 0.79-1.02, and D85E: 0.69-0.98,

230   95% confidence interval). Variants that disrupted glycosylation sequons (residues 5-7 and 26-

231   28) largely did not alter channel function despite their effects on KCNE1 trafficking (Figure S7B),

232   consistent with previous work.[26,27] Additionally, N-terminal cysteine residues, while gain-of-

233   trafficking, did not drastically affect function. This is expected, as the assay is not well-powered

234   to detect gain-of-function variants. Only one variant (Y107R) met the "gain-of-function" criteria

235   (score estimate > 97.5% percentile of synonymous scores) and was validated by manual patch

236   clamp (Figure S7C).[26,27]

237

238   ***Structural model of the KCNE1/KCNQ1/calmodulin complex***

239   An experimental structure of the KCNE1/KCNQ1/calmodulin complex has not been

240   determined, so we examined multiple AI-based models (Figure S8). Aligning predicted

241   structures of KCNE1 to a reported cryo-EM structure of the KCNQ1-KCNE3 complex indicated

242   that the conformation obtained from AlphaFold-multimer modeling (See Supplemental

243   Methods) was likely the most biologically meaningful (Figures 1A and 5). We therefore overlaid

244   mean trafficking and functional scores on the AlphaFold-multimer structural model of the

245   KCNE1-KCNQ1-calmodulin complex (Figure 5A-D). As discussed above, the hydrophobic core of

246   the transmembrane helix (residues 44 to 60) did not tolerate polar or charged variation in both

247   trafficking and function maps. Multiple variants in the cytosolic membrane-proximal region of

248   the transmembrane domain (residues 61-70) increased cell surface expression but were

249   functionally intolerant to variation. This region contains contacts with KCNQ1, including KCNE1

250   residues M62, Y65, and S68 (Figure 5F). Thus, variation in this region likely disrupts normal

251   gating properties of the I_{Ks} channel. Polar and charged variation in an additional predicted

252   intracellular helix (residues 85-105 including functionally constrained residues F78, Y81, I82,

253   and W87) preserved cell surface expression. However, the helix was functionally intolerant to

254   variation likely due to observed interaction with calmodulin (Figure 5G) that affects gating

255   properties of the I_{Ks} complex. Overall, of the 30 KCNE1 residues highly intolerant of variation

256   (>70% of missense variants at given residue position are loss-of-function), 22 (73%) were in

257   close contact (<5Å) with KCNQ1 (14 residues) and/or calmodulin (9 residues; residue 77 was in

258   close contact with both proteins). These variation-resistant residues comprise 40% of 55 KCNE1

259   residues in close contact with KCNQ1 and/or calmodulin. On the other hand, none of the 70

260   residues where >50% of the missense variants had WT-like functional scores were in close

261   contact with either KCNQ1 or calmodulin.

262

263   ***Correlation of MAVE scores with patch clamp and patient data***

264   We curated a list of 149 *KCNE1* variants with previously published patch clamp,

265   trafficking and patient data, (Additional File 1) and conducted additional patch clamp studies of

266   15 variants (Table S1). The MAVE function scores were strongly correlated with measured or

267   reported peak currents ($p = 1.5 \times 10^{-9}$, $\rho = 0.65$, n = 71; Figure 6A). 26/29 variants with ≤25% of

268   WT peak current had deleterious function scores. Only 8 of these 26 had deleterious trafficking

269   scores (30.8%; Figure S9A). 21/29 variants with >50% WT peak current had WT-like function

270   and trafficking scores. Although function scores correlated best with peak current, *KCNE1*

271   variants with large shifts in the voltage or time kinetics of activation or deactivation were also

272   more likely to have deleterious scores (Figures 6B and S9B). The trafficking scores had weaker

273   correlations with patch clamp parameters (Figures S9C and S9D). Single nucleotide variants

274   (SNVs) achieved by transversion mutations were more likely to be functionally deleterious

275   compared to variants achieved by transition mutations ($p = 2.2 \times 10^{-4}$, Wilcoxon test; Figures S9E

276   and S9F).

277   We examined the distribution of missense variant scores in presumed normal and

278   pathogenic variants, curated from gnomAD, ClinVar and our literature review of LQT5 and JLNS

279   cases. Variants achieved by more than one single SNV or not present in gnomAD tended to have

280   deleterious function scores ($p = 9.3 \times 10^{-6}$, Wilcoxon test in Figure 6B; $p = 4.6 \times 10^{-5}$, Wilcoxon test

281   in Figure 6C; and Figure S10A). Function scores were largely concordant with clinical outcomes:

282   7/7 ClinVar benign/likely benign variants and 16/19 presumed normal variants had WT-like

283   function scores; and 3/4 ClinVar pathogenic/likely pathogenic variants and 16/19 presumed

284   pathogenic variants had deleterious function scores (Figures 6D and 6E). The predictive

285   performance of MAVE scores was tested by generating receiver operator characteristic (ROC)

286   curves. The area under the ROC curve was 0.90 for function scores and 0.70 for trafficking

287   scores (Figure 6F). Function scores correlated well with several previously validated

288   computational and evolutionary metrics of variant effect (Figure S11). The predictive

289   performance of function scores was comparable to these metrics (Figure S10B). We note that

290   while computational metrics perform well for *KCNE1* variants, our MAVE data are derived from

291   direct *in vitro* data, and thus provide orthogonal information. These trends were weaker for

292   trafficking scores (Figures S12 and S13).

293   We calibrated our assay with presumed pathogenic and benign variants, following the

294   approach recommended by the ClinGen Sequence Variant Interpretation working group.[16] We

295   used the function scores for calibration because of their better correlation with clinical

296   outcomes and other metrics of disease risk. Using the ClinVar only dataset, the functional assay

297   achieved a likelihood ratio of pathogenicity (termed "OddsPath") of 13.0 for pathogenic

298   (PS3_moderate) and 0.253 for benign (BS3_supporting). Using the expanded set of presumed

299   benign and pathogenic variants, the functional assay achieved an OddsPath of 14.3 for

300   pathogenic (PS3_moderate) and 0.168 for benign (BS3_moderate).

301

302   **Discussion**

303   A majority of variants in clinically relevant genes, including *KCNE1*, are VUS, and

304   resolving the clinical significance of VUS at scale has been a major challenge in genomic

305   medicine.[11] High-throughput functional data can be deployed to reclassify as many as 89% of

306   known VUS in clinically actionable genes.[15] Loss-of-function *KCNE1* variants cause type 5 long

307   QT syndrome (LQT5) via two major mechanisms: reduced cell surface expression and/or

308   defective gating (activation of the I_{Ks} complex).[32] Our study ascertains trafficking and

309   electrophysiology properties to better understand the disease risk of nearly all possible *KCNE1*

310   variants. Furthermore, our dataset provides functional scores for 871 of the 924 *KCNE1* variants

311   accessible by a single SNV; each variant, if compatible with life, is estimated to exist in

312   approximately 50 humans currently alive.[14] Our comprehensive datasets also reveal new

313   biology not apparent from previous smaller-scale mutational studies.

314

315   ***Insights from trafficking scores***

316   We identified 470 loss-of-trafficking and 310 gain-of-trafficking missense variants,

317   including a stretch of super-trafficking N-terminal cysteine variants. We hypothesize that these

318   residues may increase cell surface expression by forming intermolecular disulfide bonds with

319   other proteins (e.g., KCNE1 or KCNQ1). We tested this hypothesis by conducting a MAVE of cell

320   surface expression in the absence of KCNQ1, but this dataset may be influenced by other low-

321   abundance binding partners of KCNE1 endogenous to HEK293T cells. Nevertheless, the result

322   clearly implicated loss of N-glycosylation at position 26, but less so at position 5, as increasing

323   cell surface expression in the presence of KCNQ1. The cell surface abundance of nonsense

324   variants in our data also highlights that the latter half of the protein (residue 56-129) is

325   dispensable for cell surface trafficking. This residue marks the beginning of the FTL domain,

326   important for electrophysiological modulation of the I_{Ks} channel,[33,34] and corresponds to a

327   previously reported kink in the transmembrane domain.[35,36]

328

329   ***Insights from function scores***

330   We developed a novel selection assay that used a gain-of-function KCNQ1 variant

331   (S140G) to identify loss-of-function KCNE1 variants. With the assay, we identified 588 loss-of-

332   function variants, of which 433 (73.7%) had normal cell surface expression. We refer to these as

333   "gating" variants, as proper K^+ flux through the I_{Ks} channel is likely disrupted. The predominance

334   of pathogenic gating variants is in contrast to other potassium channel disease genes, such as

335   *KCNH2*; 88% of 193 studied KCNH2 loss-of-function variants disrupt cell surface expression.[37]

336   The high proportion of gating variants is likely explained by KCNE1's primary function as a

337   KCNQ1-modifying subunit to modulate the I_{Ks} complex. The gating variants identified in our

338   data include well-studied variants like D76N and W87R[22] and novel variants in the

339   transmembrane-proximal cytosolic domain that interact with KCNQ1 and calmodulin. We also

340   identified gating variants predicted to interact with KCNQ1 that otherwise increase KCNE1 cell

341   surface expression. These variants likely do not disrupt intermolecular binding within the I_{Ks}

342   channel complex but are rather involved in the physical modulation of KCNQ1 with appropriate

343   electrochemical stimuli.

344   Our work defines three classes of nonsense variants based on residue location: #1-55

345   that disrupt cell surface expression, #56-104 traffic to the cell surface but do not function, and

346   #105-128 have near-normal trafficking and function.[38] While D85N (rs1805128; AF 0.14%-2.54%

347   in gnomAD) is associated with QT prolongation and fatal arrhythmias in the presence of drugs

348   and other environmental factors,[39] the variant is too common to cause long QT syndrome in

349   isolation. The WT-like MAVE score estimates are concordant with this observation (trafficking

350   score: 0.82-1.00; functional score: 0.79-1.02).

351

352   ***Structural implications of MAVE data***

353   Although there is no solved cryo-EM structure of the KCNQ1-KCNE1-calmodulin

354   complex, we used AlphaFold2 and homology modeling to construct a structural model of the I_{Ks}

355   complex. In our MAVE datasets, hydrophilic variants in the hydrophobic transmembrane core

356   (including previously studied variants like L51H)[22] disrupt function by affecting cell surface

357   expression. We also identify a 26 amino acid membrane-proximal cytosolic region (residues 61-

358   87) that comprises essential elements for I_{Ks} complex function: KCNQ1-binding and calmodulin-

359   binding regions, and a structured linker connecting the two. Variants in this region likely disrupt

360   hydrophobic and polar interactions and pi-stacking with the corresponding residues of KCNQ1

361   and calmodulin respectively. Accordingly, the region is highly constrained in the function, but

362   not trafficking, assay. With increasing confidence in and accuracy of AI-generated structural

363   models, the resolution and interpretation of MAVE-based structure-function relationships will

364   likely improve.

365

366   ***Clinical Associations of deleterious KCNE1 variants***

367   Our dataset also highlights the strength of association between *KCNE1* loss-of-function

368   variants and QT prolongation. In 2020, the ClinGen Channelopathy Working Group assessed

369 *KCNE1* as having only limited evidence for association with congenital type 5 long QT syndrome

370 (LQT5) and strong evidence for association with acquired long QT syndrome.[40] Since then,

371 several papers have further described the LQT5 risk of *KCNE1* variants. Roberts *et al.*[1] reported

372 in a multi-center review of LQT5 that *KCNE1* variants are a low penetrance cause of congenital

373 long QT syndrome. Our group has previously shown that carriers of pathogenic/likely

374 pathogenic *KCNE1* variants in the electronic MEdical Records and GEnomics (eMERGE)

375 sequencing study had longer QT intervals and higher odds of arrhythmia diagnoses and

376 phenotypes.[41] However, these variants conferred a lower risk than P/LP variants in *KCNQ1* or

377 *KCNH2* (LQT1 and LQT2). The QT prolonging effects of deleterious *KCNE1* variants has also been

378 established in both the TOPMed and UK Biobank cohorts, with effect sizes up to 15-20 ms.[42]

379 Thus, *KCNE1* loss-of-function variants appear to contribute to modest increases in baseline QT

380 interval.

381   The presence of a KCNE1 deleterious variant may not be sufficient for development of

382 the congenital LQT5 phenotype. For the QT interval to rise above a high-risk threshold, LQT5-

383 associated variant carriers may require additional genetic or environmental insults, such drug

384 exposure.[1] Based on the strong correlation between MAVE scores and functional and clinical

385 outcomes, variants identified as functionally deleterious in this study likely predispose carriers

386 to LQT5.

387

388 **MAVE data can supplement ACMG criteria**

389   Both our trafficking and function assays had excellent separation between early

390 nonsense and synonymous variants, high concordance among replicates, and strong

391   correlations with previous measurements of cell surface trafficking or patch clamp function. In

392   addition, the function MAVE dataset correlates well with patient and population cohorts, using

393   controls curated from ClinVar, literature reports, and gnomAD. Another advantage of the MAVE

394   approach is the uniformity and replication of the platform used to analyze variants, unlike

395   literature reports derived from multiple individual laboratories with low concordance.[43]

396   Because of this heterogeneity, data from literature reports cannot accurately contribute to

397   ClinGen guidelines for interpreting *in vitro* functional datasets.[16] The small number of

398   discordant variants between our assay and the literature might represent a failure of our assay

399   or of previous reports. Based on the ClinGen guidelines, function scores can be implemented at

400   the moderate level for both PS3 and BS3 criteria to aid in variant interpretation. However, given

401   the higher clinical burden of false negatives, we recommend using our scores conservatively to

402   apply BS3 at the supporting level. This work adds to the growing set of arrhythmia genes

403   previously assayed by multiplexed assays for either the full protein (KCNJ2, calmodulin)[44,45] or a

404   portion of the protein (SCN5A, KCNH2).[32,46,47]

405

406   **Limitations**

407   The MAVE function assay was not well-powered to detect gain-of-function variants. The

408   scores were generated in a heterologous system that may not fully model the behavior of the

409   I_{Ks} channel in a cardiomyocyte. Additionally, we did not model several known behaviors of the

410   I_{Ks} channel, such as regulation by PIP_2 or adrenergic stimulation. We also did not measure

411   dominant negative properties of the channel, demonstrated for some KCNE1 variants including

412   D76N.[48] HEK293T cells endogenously express non-KCNQ1 binding partners of KCNE1 that might

413   confound trends when assessing the trafficking of KCNE1, especially in the absence of KCNQ1.

414   While variants with the lowest trafficking scores uniformly had loss-of-function scores,

415   some partial loss-of-trafficking variants had non-deleterious function scores (Figure 4D). This

416   result may reflect the flexible stoichiometry of the channel. KCNE1 can bind to KCNQ1 in a 1:4

417   to 4:4 conformation.[49] Since KCNE1 is highly expressed in our assays, cells expressing partial

418   loss-of-trafficking variants may bind to KCNQ1 in higher proportions to activate KCNQ1 and

419   yield some I_{Ks} function.

420   Although KCNE1's major role in the cardiac action potential is through its role in I_{Ks},

421   KCNE1 has also been reported to interact with other proteins including KCNH2[50] and

422   TMEM16A, a cardiac chloride channel.[51] These interactions might influence arrhythmia risk that

423   is not captured by the I_{Ks} assay performed in this study. For example, previously discussed

424   variant D85N has been reported to cause a partial loss-of-function of KCNH2,[52] which may

425   explain its influence on the QT interval. An extension of this work would be to investigate the

426   influence of comprehensive KCNE1 variant libraries on other protein complexes.

427

428   **_Conclusions_**

429   We comprehensively ascertained variant function in an important arrhythmia gene,

430   _KCNE1_. We identified 470 variants that affect KCNE1 trafficking and 588 variants that alter

431   function. Our work highlights new biology of the I_{Ks} channel and can be implemented in the

432   ACMG/AMP scheme to classify variants.

433

434

435   **Declarations**

436   ***Ethics approval and consent to participate***

437   Not applicable.

438

439   ***Consent for publication***

440   Not applicable.

441

442   ***Availability of data and materials***

443   The three MAVE datasets supporting the conclusions of this article are available in Additional

444   File 2 and will be deposited in MaveDB[53] upon publication. Illumina sequence data will be

445   archived in the Short Read Archive upon publication. Code to analyze MAVE data and re-create

446   figures is available at https://github.com/GlazerLab/KCNE1_DMS.

447

448   ***Competing interests***

449   The authors declare that they have no competing interests.

450

451   ***Funding***

452   This research was funded by R00 HG010904 (AMG), R01 HL149826 (DMR), R01 HL164675

453   (DMR) and RM1 HG010461 (DMF). AM received support from the American Heart Association

454   (20PRE35180088) and the Vanderbilt Medical Scientist Training Program (T32GM007347). Flow

455   cytometry experiments were performed in the VUMC Flow Cytometry Shared Resource, which

456   is supported by the Vanderbilt Ingram Cancer Center (P30 CA68485) and the Vanderbilt

457   Digestive Disease Research Center (DK058404).

458

459   ***Author Contributions***

460   AM, DMR, and AG designed the research and wrote the manuscript. AM, MC, BL, TY, DJB, MLH,

461   JS, AEC, and AMG performed the research. AM, MC, BL, TY, DJB, JS, DMR, and AMG analyzed

462   the data. JAC, KAM, and DMF contributed essential resources and reagents. All authors

463   reviewed and approved the manuscript.

464

465   ***Acknowledgements***

466   We thank Fritz Roth, Jochen Weile, Bjorn Knollmann, David Samuels, the CardioVar consortium,

467   and members of the Vanderbilt Center for Arrhythmia and Therapeutics for helpful discussions.

468   We thank Kara Skorge, Laura Short, Marcia Blair, and Lynn Hall for cloning assistance and the

469   Vanderbilt VANTAGE sequencing core for performing Illumina sequencing.

470

471   ***Author's Twitter handles***

472   @ayeshamyar (AM), @capra_lab (JAC), @kmatreyek (KAM), @dougfowler42 (DMF),

473   @rodendm (DMR), and @amglazer (AMG)

474

475   **Methods**

476   ***Overview of multiplexed assays of KCNE1 variant effects***

477   An HA epitope tag was cloned into the extracellular region of *KCNE1*. Saturation

478   mutagenesis was used to create a plasmid library of 2,592 distinct single amino acid *KCNE1*

479   variants (95.7% of total possible variants). Each plasmid was associated with a random 18-base

480   barcode and the plasmid library was "subassembled", i.e., deep sequenced to connect each

481   barcode to its corresponding KCNE1 variant. To express one *KCNE1*-HA variant per cell, the

482   library was integrated into Human Embryonic Kidney (HEK) 293T cells engineered to include a

483   "landing pad."[18] To determine cell surface expression, *KCNE1*-HA variants were expressed with

484   or without WT *KCNQ1* and the cell pool was stained with an anti-HA antibody. Cells were sorted

485   into 4 bins based on the level of cell surface labeling, and each bin was deep sequenced to

486   quantify variants. To determine channel function, *KCNE1-HA* variants were expressed with a

487   gain-of-function *KCNQ1* variant for 20 days to deplete cells with normally functioning I_{Ks}

488   channels. The cell pool was deep sequenced at day 0, 8 and 20 to quantify variants (Figure S1).

489

490   ***Cloning a novel KCNE1 HA tag***

491   We used *KCNE1* (NCBI Reference Sequence NM_001127670.4) with the G allele at residue 38

492   (p.S38G, c.112A>G, rs1805127), as this variant allele is more common globally (65.8% allele

493   frequency [AF] across all ancestral populations in gnomAD; range 57.4%-71.3%).[54] An HA

494   epitope (5'-TACCCCTACGATGTACCAGATTATGCG-3') was cloned between residues 34 and 35

495   with primers ag424 and ag425 using inverse PCR with Q5 polymerase (New England Biolabs,

496   NEB).[23] The sequences of all primers used in this study are presented in Table S2. The resulting

497   gene, *KCNE1*-HA, was subcloned into the pIRES2-dsRED2 plasmid using PCR with ag409 and

498   ag410 and NotI restriction digestion (NEB) to create *KCNE1*-HA:pIRES2:dsRED2. All plasmid

499   sequences were verified with Sanger sequencing. Using NotI restriction digestion, the *KCNE1-*

500   HA gene was moved to an AttB plasmid containing pIRES:mCherry:BlastR to create p*KCNE1-*

501   HA:IRES:mCherry:BlastR. We also used a compact (<4kb) promoterless plasmid for single-

502   variant mutagenesis.[46] Maps of key plasmids used in this study are shown in Figure S14A.

503

504   *Generation of HEK293T lines stably expressing KCNQ1 or KCNQ1-S140G*

505   The experiments were conducted in either previously published Bxb1-mediated landing pad

506   HEK293T (LP) cells,[18] or LP cells genetically engineered to express *KCNQ1* (WT or S140G). LP

507   cells contain an AttP integration "landing pad," Blue Fluorescent Protein (BFP), and iCasp9

508   caspase downstream of a doxycycline-induced promoter.[18] The AttB:mCherry:BlastR plasmid

509   integrates into the AttP landing pad. Prior to integration, the promoter drives BFP and iCasp9

510   expression. After integration, the promoter drives expression of mCherry and blasticidin

511   resistance genes instead. Cells with a successful plasmid integration event are blasticidin

512   resistant, express mCherry and lack iCasp9, which can be used to select for recombined cells.

513   Genetically engineered LP cells expressing KCNQ1 (WT or S140G) were generated as below.

514

515   Since the plasmids use NotI restriction digestion for subcloning, we removed an intra-cDNA

516   NotI restriction enzyme site, by introducing a synonymous mutation (c.246G>T), into WT

517   *KCNQ1* cDNA (NM_000218.3) using QuikChange mutagenesis (Agilent). The *KCNQ1* gain-of-

518   function variant (p.S140G, c.418A>G, rs120074192) was also generated by QuikChange

519   mutagenesis. KCNQ1 S140G biases I_{Ks} channels to the open state[29,31] at lower membrane

520 potentials (including the resting potential of HEK293T cells, approximately -25 mV)[28] and leads

521 to increased cellular K^+ efflux.[55]

522

523 To construct a cell line with constitutive *KCNQ1* expression, *KCNQ1* (WT or p.S140G) was cloned

524 into a Sleeping Beauty transposon system, pSBbi-GN (a gift from Eric Kowarz, Addgene#

525 60517),[56] using SfiI restriction digestion (NEB) to create pSBbi-GN::KCNQ1. This plasmid

526 expresses *KCNQ1* and *EGFP* via constitutively active bidirectional promoters. The plasmid was

527 randomly integrated into a non-landing pad locus in the LP cells with the Sleeping Beauty

528 transposase as follows. Cells were cultured at 37° at 5% CO_2 in HEK media: 10% FBS (Corning),

529 1% non-essential amino acids (Corning), 1% penicillin/streptomycin (Corning) in DMEM

530 (Thermo). On day 0, pSBbi-GN::KCNQ1 was transfected into the LP cell line along with a plasmid

531 expressing the Sleeping Beauty transposase, pCMV(CAT)T7-SB100 (a gift from Zsuzsanna Izsvak,

532 Addgene #34879),[57] using FuGENE6 (Promega) in a 1:3 ratio with DMEM. On day 6, the cells

533 were exposed to HEK media with 1 μg/mL doxycycline (Sigma) to induce expression of the

534 BFP/iCasp9 from the landing pad. The cells were sorted with a BD FACSAria IIIU (BD

535 Biosciences), using a 100 μm nozzle for cells with high levels of BFP and high levels of GFP

536 (Figure S14B) into HEK media on amine-coated plates (Corning). Single-cell colonies were grown

537 in HEK media, with the addition of 1 μg/mL doxycycline 48 hours before being screened on a BD

538 LSRFortessa SORP (BD Biosciences) to identify colonies with high rates of both landing pad (*BFP*)

539 and *KCNQ1* (*GFP*) expression (Figure S14C). Two distinct colonies with high blue and green

540 fluorescence were expanded for further experiments. The landing pad cell line expressing WT

541   KCNQ1 is referred to as LP-KCNQ1 and the cell line expressing KCNQ1 S140G is referred to as

542   LP-KCNQ1-S140G.

543

544   For transient transfection experiments, plasmids that constitutively expressed *KCNE1* or *KCNQ1*

545   were cloned using NotI restriction digestion into pIRES2:EGFP or pIRES2:dsRED2 to create all

546   four combinations: p*KCNE1*:IRES:EGFP, p*KCNE1*:IRES:dsRED2, p*KCNQ1*:IRES:EGFP, and

547   p*KCNQ1*:IRES:dsRED2 (see Supplemental Methods for more details).

548

549   **KCNE1 library creation**

550   Each of the 129 *KCNE1* residues was comprehensively mutated using inverse PCR on the

551   compact template plasmid.[23,46] For each mutagenesis reaction, the forward primers contained a

552   5' degenerate NNK sequence for each codon to introduce all 20 sense amino acid variants and 1

553   nonsense variant at each site. The 129 PCR reactions were pooled, PCR-purified (QIAGEN),

554   phosphorylated with T4 PNK (NEB), and self-ligated using T4 ligase (NEB). The pooled product

555   was re-PCR-purified and electroporated into ElectroMAX DH10B Cells (ThermoFisher) using a

556   Gene Pulser Electroporator (Bio-Rad; 2.0 kV, 25 μF, 200 Ω). Serial dilutions of the

557   electroporated cells were plated on Ampicillin plates to determine transformation efficiency.

558   The library was purified using a MaxiPrep kit (Qiagen) and subcloned into a promoterless AttB

559   pIRES:mCherry-BlastR[18,46] plasmid using restriction digestion with AatII and AflIII (NEB). The

560   library was then re-electroporated and purified as above.

561   For quantification, each variant construct was tagged with a random 18mer barcode to

562   the library plasmid. The barcode was generated using ag289 (spacer-BsiWI-AflIII-N18-AatII-XbaI-

563   spacer) and ag290 (reverse complement of the 3' end of ag289). The two primers were

564   annealed by incubating at 95° for 3 minutes and cooling by 1°/10 s. The annealed primers were

565   extended to fully double stranded DNA using Klenow polymerase (NEB). The barcode was

566   purified by phenol-chloroform extraction, digested with BsiWI and XbaI (Thermo Fisher), and

567   re-purified by phenol-chloroform extraction. The resulting DNA fragment was ligated into the

568   *KCNE1*-HA plasmid library. The plasmid library was deep sequenced to link each barcode to its

569   associated variant (see Supplemental Methods). A map of the final barcoded plasmid library

570   (p*KCNE1*-HA library:pIRES:dsRed:BlastR) is provided in Figure S3A.

571

572   ***Integration of library into landing pad cells***

573   LP, LP-KCNQ1, or LP-KCNQ1-S140G cells were cultured in 10 cm dishes in HEK media until

574   approximately 60% confluent. Cells were then transfected with 25 µg of p*KCNE1*-HA

575   library:IRES:dsRed:BlastR and 5µg of site-specific recombinase, pCAG-NLS-HA-Bxb1 (a gift from

576   Pawel Pelczar, Addgene #51271)[58] using Lipofectamine 2000 (Thermo Fisher) in a 1:2 ratio.[18] 6-

577   8 hours after transfection, the cells were fed fresh media. The following day, cells were

578   passaged using Accutase (Sigma) into two 10 cm dishes and fed media supplemented with 1

579   µg/mL doxycycline (Sigma) to induce expression of the landing pad. With successful integration

580   of a single AttB-containing plasmid, the landing pad expresses only one *KCNE1*-HA variant,

581   mCherry, and BlastR. 24 hours later, cells were singularized in place using 1 mL Accutase,

582   quenched with 10 mL selection media (HEK media as above with 1 µg/mL doxycycline, 100

583   µg/mL blasticidin (Sigma), and 10nM AP1903 (MedChemExpress)). Addition of blasticidin and

584   AP1903   selected   for   successfully   integrated   cells   that   expressed   *KCNE1*-HA

585   library:pIRES:mCherry:BlastR and against non-integrated cells that continued to express

586   BFP/iCasp9 caspase. Cells were grown in selection media for 8 days post-transfection. For the

587   LP-KCNQ1-S140G line, cells with successful integration were enriched in HEK selection media

588   containing a high concentration (500 nM) of the HMR 1556 (Tocris), a specific I_{Ks} blocker with

589   an IC_{50} of 10.5 nM.[59]

590

591   *Trafficking assay*

592   We measured cell surface trafficking of the *KCNE1*-HA library in the presence and absence of

593   *KCNQ1*, using LP-KCNQ1 and LP cells, respectively. Each experiment was performed in triplicate

594   (three independently transfected, stained, sorted, and sequenced replicates).

595   To stain KCNE1-HA at the cell surface, day 8 post-selection, cells were dissociated using

596   Accutase and quenched with HEK selection media. For any subsequent cellular suspension, cells

597   were centrifuged for 5 minutes at 300 g and suspended in the new solution. The cells were

598   washed with block solution (1% FBS +25 mM HEPES pH 7.0 [Sigma] in PBS without Ca^{2+}/Mg^{2+}).

599   The cells were then stained with 1:500 anti-HA AF647 conjugated antibody (Cell Signaling

600   #3444) in block solution for 45 minutes at room temperature in the dark and washed three

601   times. Stained cells were resuspended in block solution at a concentration of 4-6 million

602   cells/mL for sorting. Two trafficking experimental replicates were performed with cells in

603   suspension as described above. One replicate was stained while cells were adhered on the dish

604   (see Supplemental Methods).

605   Stained cells were FACS sorted on the BD FACSAria III (BD Biosciences) using a 100 µm

606   nozzle. Compensation was performed using cells expressing single fluorophores or AF647

607   compensation beads (Thermo Fisher). Single cells were identified based on forward and side

608   scatter signals. BFP$^-$/mCherry$^+$ single cells (with and without GFP for *KCNE1* with and without

609   *KCNQ1* experiments, respectively) were divided into 4 groups of approximately equal size based

610   on AF647 labeling (Figure S15). At least 800,000 cells per group were sorted and replated onto

611   amine-coated plates containing HEK media. Cells were expanded and genomic DNA was

612   extracted from each group with the Quick-DNA midiprep kit (Zymo). Q5 polymerase was used

613   to amplify the barcodes from gDNA with 20 cycles of amplification using Illumina-compatible

614   primer pairs (Table S2), and the barcodes were sequenced on the Illumina NovaSeq PE150 with

615   at least 25 million reads per sample. Normalized cell surface trafficking scores were calculated

616   from a weighted average of barcode counts from these samples (see Supplemental Methods for

617   details).

618

619   ***Cell fitness assay***

620   The cell fitness assay was validated by 1:1 competition experiments on control variants (see

621   Supplemental Methods for details) and then conducted on the entire library. The

622   comprehensive library was integrated into the landing pad of cells as described above. Fitness

623   of cells expressing *KCNE1*-HA variants in the library was measured in LP-KCNQ1-S140G in three

624   independent replicates. 8 days after successful plasmid integration, termed Day 0 in

625   subsequent analyses, cells were washed with selection media to remove HMR 1556, and a

626   subset of cells harvested for gDNA extraction. Cells were passaged as needed. Additional

627   samples were harvested for gDNA extraction on Day 8 and Day 20. Genomic DNA from these

628   three time points (Days 0, 8 and 20) was isolated. Barcode pools were amplified and sequenced

629   using the Illumina NovaSeq as described above.

630

631   **Population-level analyses**

632   The data for putative controls were obtained from gnomAD v.2.1.1 (exomes and genomes,

633   accessed October 2022).[54] Variant annotations were obtained from the ClinVar database

634   (accessed October 2022).[13] In addition, we performed a literature review that consisted of a

635   PubMed search (on November 30, 2022) for "KCNE1." The resulting 929 manuscript titles and

636   abstracts were manually reviewed to collate published patch clamp electrophysiology and

637   patient data (Additional File 1, see Supplemental Methods for more details). Variants in at least

638   1 patient with LQT5 (Romano-Ward or one allele of JLNS) and an AF $< 2.5 \times 10^{-5}$ across all

639   ancestries in gnomAD were classified as putative LQT5-associated variants. Similarly, the 2

640   variants previously seen in cases with atrial fibrillation, G25V and G60D, also had allele

641   frequencies $< 2.5 \times 10^{-5}$, and thus were classified as putative atrial fibrillation-associated variants.

642   Putative benign variants had an estimated penetrance of $< 10\%$ ($\frac{\#}{\# + \;}$) and had an allele

643   frequency of $> 3 \times 10^{-5}$ in gnomAD. Only 1 variant (G55S) with an allele frequency of $> 3 \times 10^{-5}$ had

644   a penetrance of $> 10\%$ and was excluded.

645

646   **ACMG Assay Calibration**

647   Missense variants classified in ClinVar as pathogenic/likely pathogenic or in our curated list of

648   putative LQT5 variants were classified as "presumed cases." Missense variants classified as

649   benign/likely benign in ClinVar or in our curated list of putative normal variants were classified

650   as "presumed controls". Variants with score estimates (mean and 95% confidence interval)

651   below the 2.5[th] percentile or above the 97.5[th] percentile of the synonymous distribution were

652   defined as loss-of-function and gain-of-function respectively. Variants with score estimates

653   within the cutoffs were classified as "functionally WT-like." Missense variants score estimates

654   that overlapped the cutoffs were classified as "indeterminate." Only one variant (Y107R) had a

655   function score estimate higher than the 97.5[th] percentile cutoff. To determine the strength of

656   evidence at which MAVE scores could be used as evidence for the ACMG functional assay

657   criteria (PS3/BS3), the assay OddsPath was calculated using previously described methods.[16]

658
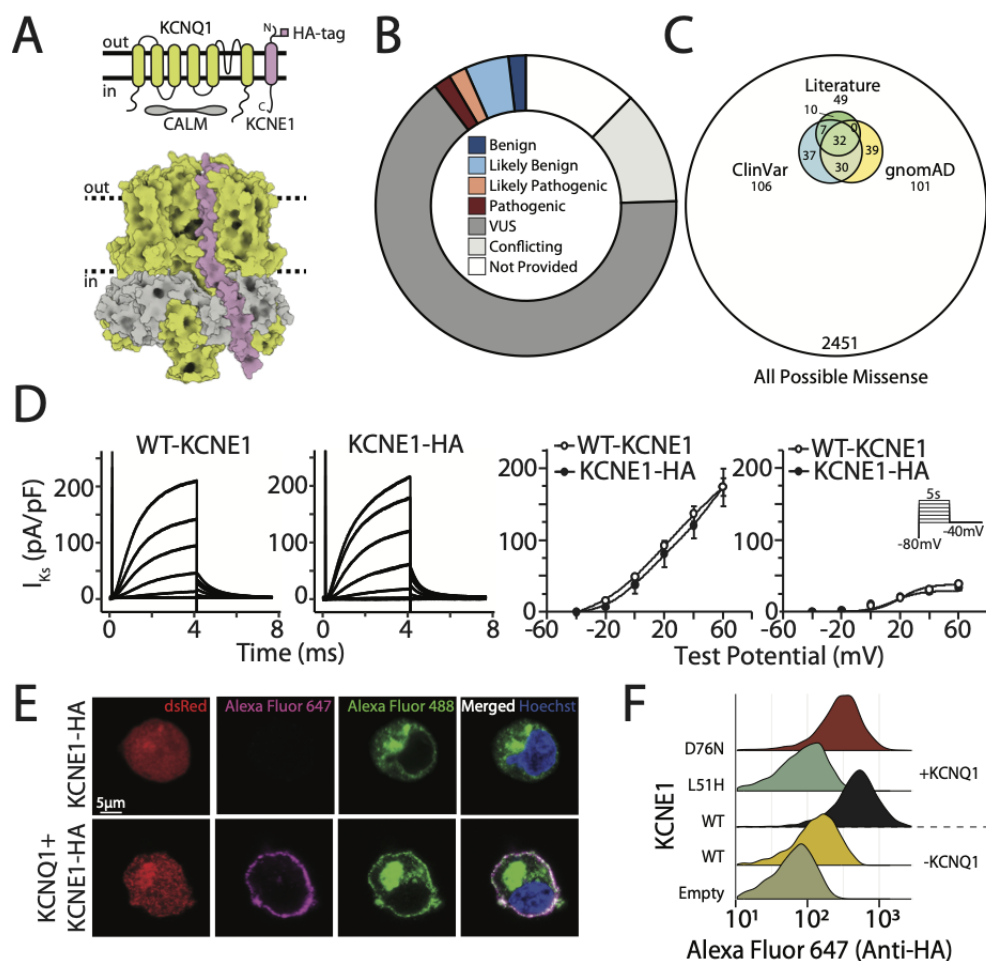
659

660 **Figure 1: Overview of the I_{Ks} channel and a novel location for the HA epitope**

661 A) The I_{Ks} channel complex is formed by KCNE1 (pink), KCNQ1 (green), and calmodulin (gray;

662 top: schematic, and bottom: three-dimensional structure). The HA tag in KCNE1 (cloned

663 between residues 34 and 35) is labeled. B) Most of the 106 missense KCNE1 variant

664 classifications in the ClinVar database are VUS or conflicting (Figure style adapted from Starita

665 et al., 2017). C) Variants reported in ClinVar, gnomAD, and previous studies comprise a small

666 portion of all possible KCNE1 missense variants. D) The HA tag did not disrupt I_{Ks} (left:

667 representative traces, inset: voltage protocol, and right: quantification of peak and tail current;

668 n=4 cells/condition). E) An HA tag was used to visualize KCNE1. Live HEK293T cells were stained

669 with an Alexa Fluor 647-conjugated anti-HA antibody to detect surface KCNE1, then fixed,

670 permeabilized, and stained with an Alexa Fluor 488-conjugated anti-HA antibody to detect total

671 KCNE1. dsRed is the KCNQ1 and KCNE1 transfection marker. Cells expressing only KCNE1-HA

672 showed minimal surface labeling in the absence of KCNQ1 (top). Cells expressing KCNE1-HA and

673 KCNQ1 had normal cell surface expression (bottom). F) Live cells stained for extracellular

674 KCNE1-HA had minimal but detectable labeling in the absence of KCNQ1, but 6.1-fold higher

675 labeling in the presence of KCNQ1. Known trafficking-null variant (L51H) had minimal cell

676 surface expression, but a known gating variant (D76N) had near-wild type cell surface

677 expression.

678

679
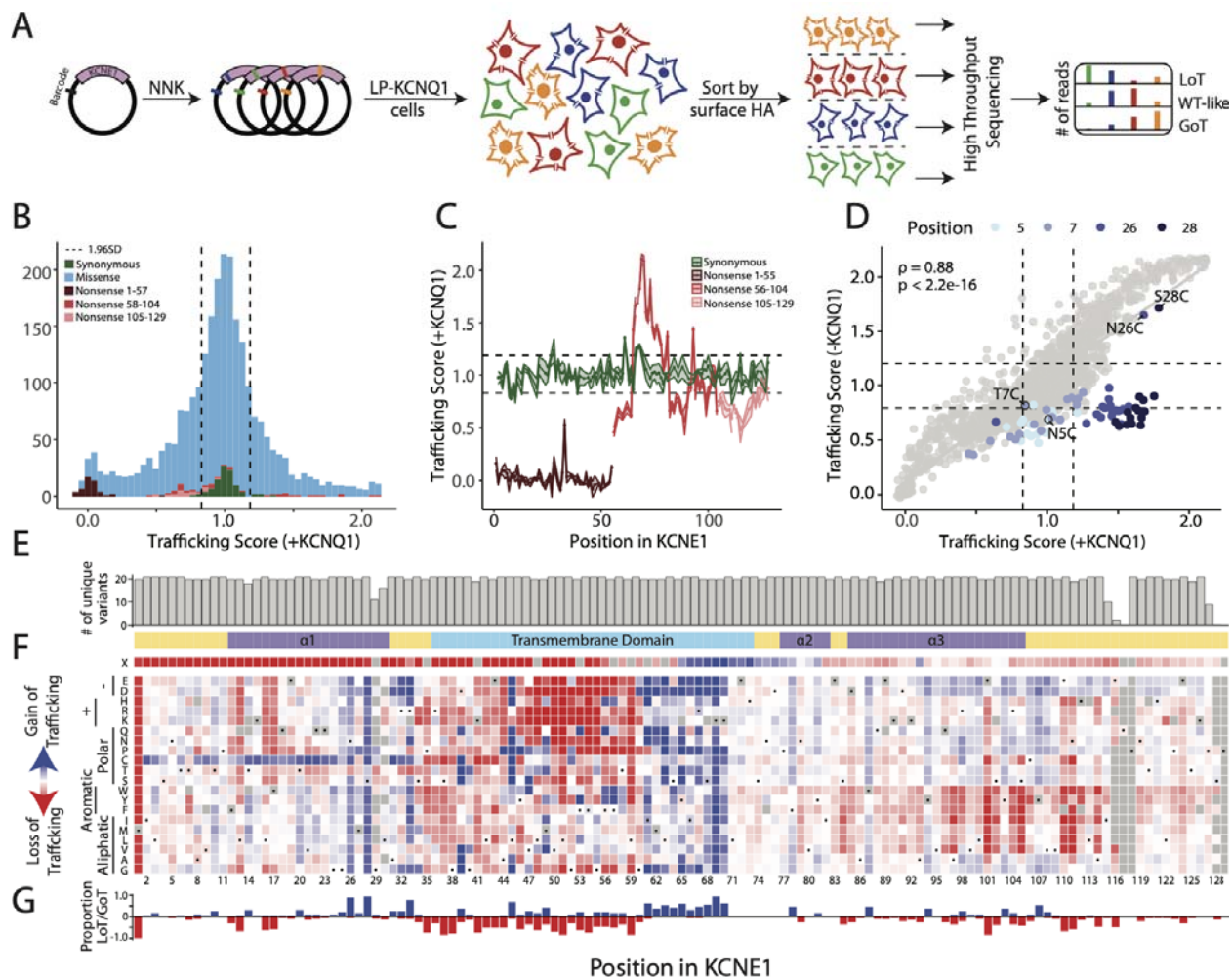
Figure 2: Multiplexed assay of _KCNE1_ cell surface expression

A) To conduct the cell surface expression multiplexed assay of _KCNE1_, a comprehensively mutated barcoded plasmid pool was integrated into the LP-KCNQ1 cell line. Cells were stained and sorted by surface KCNE1 levels and deep sequenced. B) Histogram of normalized trafficking scores by functional class showed a unimodal distribution of missense variant scores centered at the median of synonymous variant scores. A smaller peak at the median of early nonsense variant scores and a tail of super-trafficking variant scores was also seen (Dotted lines: mean ± 1.96 SD for the synonymous distribution). C) Most nonsense variants (1 per residue) from residues 1-55 (brown) are loss-of-trafficking but nonsense variants after residue 55 (red or pink)

689   are gain-of-trafficking or WT-like. Synonymous variants (1 per residue) are represented in green

690   (Dotted lines: mean ± 1.96 SD for the synonymous distribution). D) Trafficking scores in the

691   presence and absence of KCNQ1 were highly correlated with the exception of variants at

692   residues 5, 7, 26, and 28 which disrupted glycosylation sequons (highlight). Cysteine variants at

693   these sequons did not follow this trend (annotation). See Figure S5 for a full description of the

694   KCNQ1⁻ trafficking assay (Dotted lines: mean ± 1.96 SD for the synonymous distribution). E)

695   Near complete representation of variants was scored at each position in the KCNE1 protein

696   (max = 21). F) A heatmap showing trafficking scores. Red, white, and blue indicate low, WT-like,

697   and high cell surface expression, respectively. WT amino acids are indicated at each position

698   with a dot. The colored ribbon indicates secondary structure, (purple = alpha helices, light blue

699   = transmembrane domain, yellow = unstructured regions). G) For each residue, the proportion

700   of gain-of-trafficking (GoT) and loss-of-trafficking (LoT) missense variants is displayed.

701
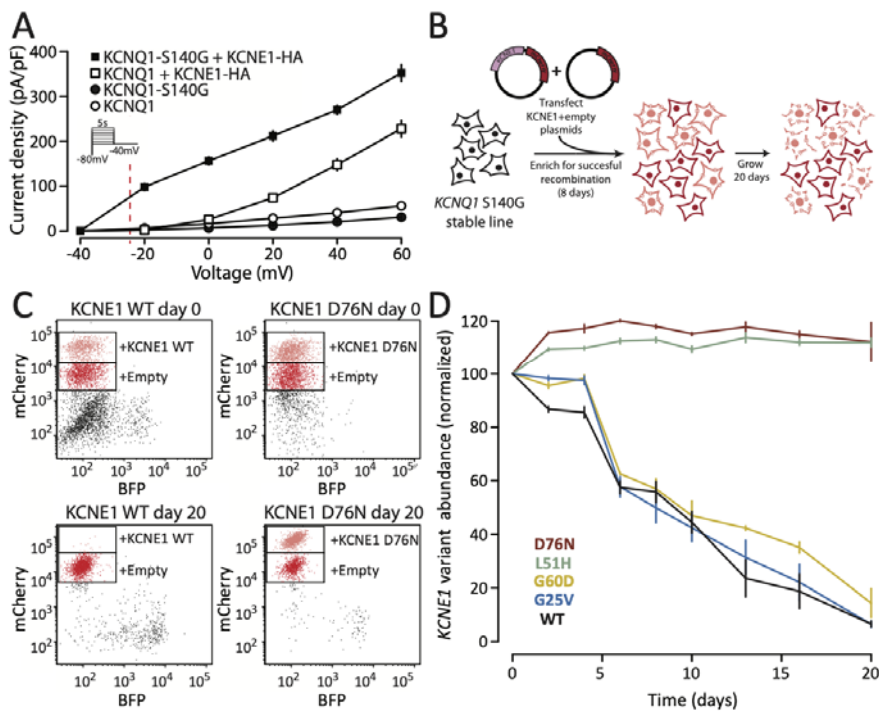
702 **Figure 3: A KCNE1 function assay using a gain-of-function KCNQ1 variant**

703 A) Voltage clamp measurements of outward potassium currents in HEK293T cells transfected

704 with various combinations of WT or S140G KCNQ1 and/or KCNE1-HA. At the resting potential of

705 HEK293T cells (~ -25 mV, dotted line), there is almost no potassium current in cells transfected

706 with KCNQ1 ± KCNE1-HA. However, the gain-of-function KCNQ1-S140G variant results in a

707 leftward shift of voltage of activation and increased current at -25 mV, only in the presence of

708 KCNE1. B) Experiment to validate KCNE1 selection assay using LP-KCNQ1-S140G cells

709 transfected with 1:1 pools of KCNE1 variant and empty vector plasmids. C) Representative flow

710 cytometry measurements of cells transfected with 1:1 pools of plasmids. Cells with empty

711 vectors had reduced mCherry fluorescence allowing quantification of distinct cell populations.

712 After 20 days of selection, there was a strong depletion of cells expressing KCNE1-HA-WT but

713 not a loss-of-function variant D76N. D) Time course of relative fitness of cells expressing KCNE1

714 variants compared to cells expressing empty vectors. All values are normalized to the values at

715 day 0. Cells expressing KCNE1-HA-WT or two gain-of-function variants (G25V and G60D)

716 depleted over 20 days but cells expressing two loss-of-function variants (D76N and L51H)

717 persisted in the cell pool. Points and error bars indicate mean and standard error of three

718 replicates.

719

720
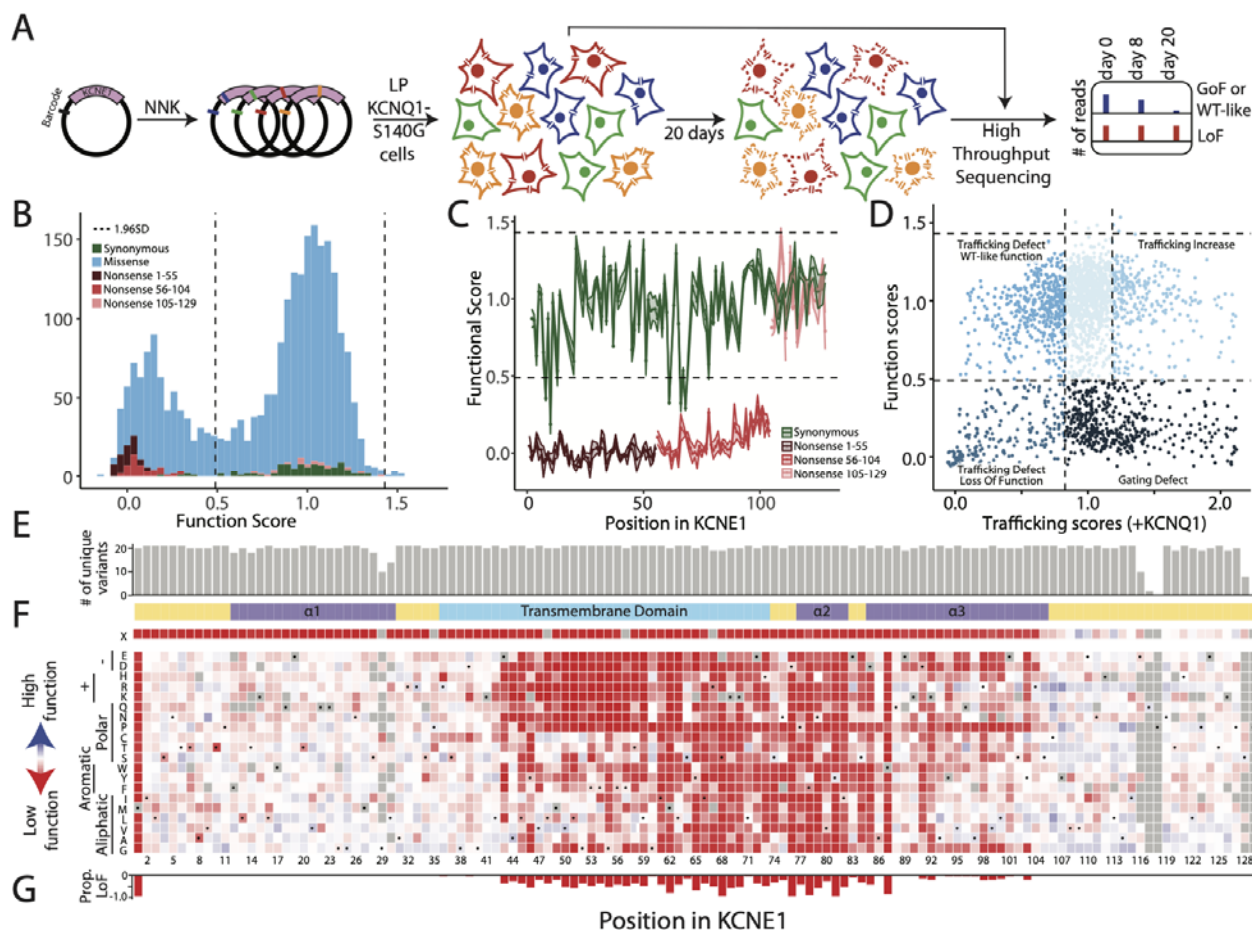
Figure 4: Multiplexed assay of _KCNE1_ function

A) Schematic of multiplexed assay of _KCNE1_ function. A comprehensively mutated barcoded plasmid pool was integrated into LP-KCNQ1-S140G cells. Cells were grown for 20 days and cell pools at 0 days, 8 days, and 20 days were deep sequenced. B) Histogram of normalized functional scores by functional class showed a bimodal distribution of missense variants (Dotted lines: mean±1.96 SD for the synonymous distribution). C) Nonsense variants (1 per residue) up to residue 104 are functionally deleterious (brown and red), including residues 56-104 that were dispensable for cell surface trafficking (red). Synonymous variants (1 per residue) are represented in green (Dotted lines: mean ± 1.96 SD for the synonymous distribution). D) Relationship between trafficking and function scores for missense variants showed that most

731   deleterious variants disrupt gating (Dotted lines: mean ± 1.96 SD for the synonymous

732   distribution). E) Near complete representation of missense variants was scored at each position

733   in KCNE1 (max = 21). F) KCNE1 function score heatmap. Red, white, and blue indicate loss-of-

734   function, normal function, and gain-of-function, respectively. WT amino acids are indicated at

735   each position with a dot. The colored ribbon indicates secondary structure as in Figure 2. G) For

736   each residue, the proportion of loss-of-function missense variants is displayed.

737
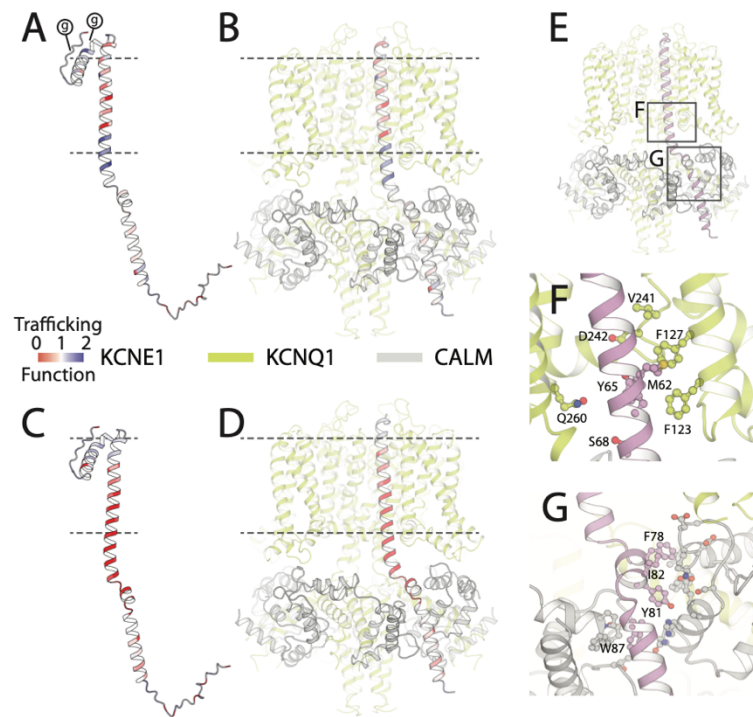
738

739   **Figure 5: Structural impact of variant effects**

740   A-D) KCNE1 structural model, coded by mean trafficking scores (A,B) or function scores (C,D) at

741   each residue on the same color scale as in Figures 2F and 4F (Red = loss-of-trafficking/function,

742   white = WT-like, blue = gain-of-trafficking/function). Dotted lines indicate the approximate

743   location of the plasma membrane. (g) represents glycosylation sites. Panels B and D show

744   KCNE1 in complex with KCNQ1 (green) and calmodulin (gray). E) I_{Ks} complex showing locations

745   of panels F and G. F) Constrained KCNE1 residues (pink) that make contacts with KCNQ1. KCNE1

746   residue M62 forms a hydrophobic cluster with KCNQ1 residues F123, F127 and V241, whereas

747   KCNE1 residues Y65 and S68 make polar contacts with KCNQ1 residues D242 and Q260,

748   respectively. G) Constrained KCNE1 residues (pink; F78, Y81, I82, W87) that make contacts with

749   calmodulin. Residues on calmodulin not labeled.

750
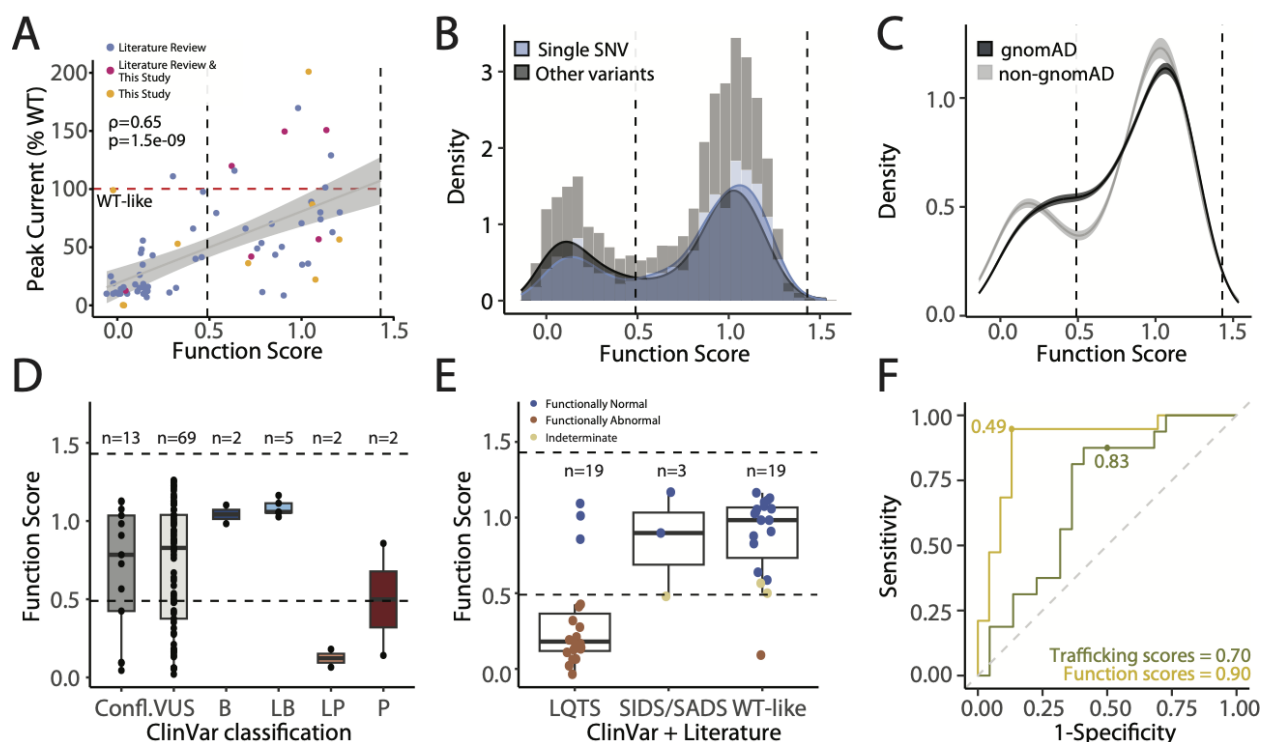
751

752   **Figure 6: Function scores correlate with *in vitro* assays and clinical outcomes**

753   A) Correlation of function scores with peak current (normalized to WT) from patch clamp

754   studies. Blue: literature review, pink: literature review and this study, yellow: this study. B)

755   Single SNV variants (blue) are less likely to have deleterious function scores compared to all

756   other variants (black; p = 9.3×10^{-6}, Wilcoxon Test). C) Variants present in gnomad (black) were

757   more likely to have WT-like scores than variants absent from gnomAD (grey; $p=2.2\times10^{-4}$,

758   Wilcoxon Test). Mean and confidence intervals are generated by re-sampling both distributions

759   100 times. D) Function scores by ClinVar classification. E) Function scores for presumed control

760   and presumed disease-associated variants. See Additional File 1 for the literature review

761   dataset. F) Receiver operator characteristic curves evaluating prediction of variant

762   pathogenicity by function and trafficking scores. Dots indicate the deleteriousness cutoffs used

763   in this study (functional scores = 0.49, trafficking scores = 0.83). The area under the curve is

764   listed at the bottom of the panel.

765

766   **Additional files**

767   Additional File 1: Literature review of KCNE1 variants. File name: AdditionalFile_LitRev.csv

768   Additional File 2: Function and trafficking scores for KCNE1 variants. File name:

769   AdditionalFile_MAVEscores.csv

770   Additional File 3: Structure of the KCNE1/KCNQ1/calmodulin complex with mean function

771   scores at each residue overlaid on KCNE1. File name: KCNE1-AF2-full-func-score-mapped.pdb

772   Additional File 4: Structure of the KCNE1/KCNQ1/calmodulin complex with mean trafficking

773   scores at each residue overlaid on KCNE1. File name: KCNE1-AF2-full-traffick-score-mapped.pdb

774   Additional File 5: Computational scores curated for variants tested in this study. File name:

775   AdditionalFile_CompScores.csv

776

777   **References**

778   1.   Roberts, J. D. *et al.* An International Multicenter Evaluation of Type 5 Long QT Syndrome: A Low

779   Penetrant Primary Arrhythmic Condition. *Circulation* **141**, 429–439 (2020).

780   2.   Splawski, I., Tristani-Firouzi, M., Lehmann, M. H., Sanguinetti, M. C. & Keating, M. T. Mutations in

781   the hminK gene cause long QT syndrome and suppress IKs function. *Nat. Genet.* **17**, 338–340

782   (1997).

783   3.   Schulze-Bahr, E. *et al.* KCNE1 mutations cause jervell and Lange-Nielsen syndrome. *Nat. Genet.* **17**,

784   267–268 (1997).

785   4.   Splawski, I. *et al.* Spectrum of mutations in long-QT syndrome genes. KVLQT1, HERG, SCN5A,

786   KCNE1, and KCNE2. *Circulation* **102**, 1178–1185 (2000).

787   5.   Westenskow, P., Splawski, I., Timothy, K. W., Keating, M. T. & Sanguinetti, M. C. Compound

788   mutations: a common cause of severe long-QT syndrome. *Circulation* **109**, 1834–1841 (2004).

789   6.   Kapplinger, J. D. *et al.* Spectrum and prevalence of mutations from the first 2,500 consecutive

790   unrelated patients referred for the FAMILION long QT syndrome genetic test. *Heart Rhythm* **6**,

791   1297–1303 (2009).

792   7.   Olesen, M. S. *et al.* Mutations in the potassium channel subunit KCNE1 are associated with early-

793   onset familial atrial fibrillation. *BMC Med. Genet.* **13**, 24 (2012).

794   8.   Yus-Najera, E., Santana-Castro, I. & Villarroel, A. The identification and characterization of a

795   noncontinuous calmodulin-binding site in noninactivating voltage-dependent KCNQ potassium

796   channels. *J. Biol. Chem.* **277**, 28545–28553 (2002).

797   9.   Harmer, S. C., Wilson, A. J., Aldridge, R. & Tinker, A. Mechanisms of disease pathogenesis in long

798   QT syndrome type 5. *Am. J. Physiol. Cell Physiol.* **298**, C263-73 (2010).

799   10.   Richards, S. *et al.* Standards and guidelines for the interpretation of sequence variants: a joint

800   consensus recommendation of the American College of Medical Genetics and Genomics and the

801   Association for Molecular Pathology. *Genet. Med.* **17**, 405–424 (2015).

802   11.   Green, E. D. *et al.* Strategic vision for improving human health at The Forefront of Genomics.

803   *Nature* **586**, 683–692 (2020).

804   12.   Starita, L. M. *et al.* Variant Interpretation: Functional Assays to the Rescue. *Am. J. Hum. Genet.* **101**,

805   315–325 (2017).

806   13.   Landrum, M. J. *et al.* ClinVar: improving access to variant interpretations and supporting evidence.

807   *Nucleic Acids Res.* **46**, D1062–D1067 (2018).

808   14.   Weile, J. & Roth, F. P. Multiplexed assays of variant effects contribute to a growing genotype-

809   phenotype atlas. *Hum. Genet.* **137**, 665–678 (2018).

810   15.   Fayer, S. *et al.* Closing the gap: Systematic integration of multiplexed functional data resolves

811   variants of uncertain significance in BRCA1, TP53, and PTEN. *Am. J. Hum. Genet.* **108**, 2248–2258

812   (2021).

813   16.   Brnich, S. E. *et al.* Recommendations for application of the functional evidence PS3/BS3 criterion

814   using the ACMG/AMP sequence variant interpretation framework. *Genome Med.* **12**, 3 (2019).

815   17.   Fowler, D. M. & Fields, S. Deep mutational scanning: a new style of protein science. *Nat. Methods*

816   **11**, 801–807 (2014).

817   18.   Matreyek, K. A., Stephany, J. J. & Fowler, D. M. A platform for functional assessment of large

818   variant libraries in mammalian cells. *Nucleic Acids Res.* **45**, e102 (2017).

819   19.   Wang, K. W. & Goldstein, S. A. Subunit composition of minK potassium channels. *Neuron* **14**, 1303–

820   1309 (1995).

821   20.   Jiang, M. *et al.* Dynamic partnership between KCNQ1 and KCNE1 and influence on cardiac IKs

822   current amplitude by KCNE2. *J. Biol. Chem.* **284**, 16452–16462 (2009).

823   21.   Chandrasekhar, K. D., Bas, T. & Kobertz, W. R. KCNE1 subunits require co-assembly with K+

824   channels for efficient trafficking and cell surface expression. *J. Biol. Chem.* **281**, 40015–40023

825   (2006).

826   22.   Bianchi, L. *et al.* Cellular dysfunction of LQT5-minK mutants: abnormalities of IKs, IKr and trafficking

827   in long QT syndrome. *Hum. Mol. Genet.* **8**, 1499–1507 (1999).

828   23.   Jain, P. C. & Varadarajan, R. A rapid, efficient, and economical inverse polymerase chain reaction-

829   based method for generating a site saturation mutant library. *Anal. Biochem.* **449**, 90–98 (2014).

830   24.   Rocheleau, J. M., Gage, S. D. & Kobertz, W. R. Secondary structure of a KCNE cytoplasmic domain.

831   *J. Gen. Physiol.* **128**, 721–729 (2006).

832   25.   Wu, D.-M. *et al.* Characterization of an LQT5-related mutation in KCNE1, Y81C: implications for a

833   role of KCNE1 cytoplasmic domain in IKs channel function. *Heart Rhythm* **3**, 1031–1040 (2006).

834   26.   Chandrasekhar, K. D. *et al.* O-glycosylation of the cardiac I(Ks) complex. *J. Physiol.* **589**, 3721–3730

835   (2011).

836   27.   Bas, T. *et al.* Post-translational N-glycosylation of type I transmembrane KCNE1 peptides:

837   implications for membrane protein biogenesis and disease. *J. Biol. Chem.* **286**, 28150–28159

838   (2011).

839   28.   Kirkton, R. D. & Bursac, N. Engineering biosynthetic excitable tissues from unexcitable cells for

840   electrophysiological and cell therapy studies. *Nat. Commun.* **2**, 300 (2011).

841   29.   Chen, Y.-H. *et al.* KCNQ1 gain-of-function mutation in familial atrial fibrillation. *Science* **299**, 251–

842   254 (2003).

843   30.   Peng, G., Barro-Soria, R., Sampson, K. J., Larsson, H. P. & Kass, R. S. Gating mechanisms underlying

844   deactivation slowing by two KCNQ1 atrial fibrillation mutations. *Sci. Rep.* **7**, 45911 (2017).

845   31.   Restier, L., Cheng, L. & Sanguinetti, M. C. Mechanisms by which atrial fibrillation-associated

846   mutations in the S1 domain of KCNQ1 slow deactivation of IKs channels. *J. Physiol.* **586**, 4179–4191

847   (2008).

848   32.   Kozek, K. A. *et al.* High-throughput discovery of trafficking-deficient variants in the cardiac

849   potassium channel KV11.1. *Heart Rhythm* **17**, 2180–2189 (2020).

850   33.   Melman, Y. F., Domènech, A., de la Luna, S. & McDonald, T. V. Structural determinants of KvLQT1

851 control by the KCNE family of proteins. *J. Biol. Chem.* **276**, 6439–6444 (2001).

852 34. Melman, Y. F., Krumerman, A. & McDonald, T. V. A Single Transmembrane Site in the KCNE-

853 encoded Proteins Controls the Specificity of KvLQT1 Channel Gating *. *J. Biol. Chem.* **277**, 25187–

854 25194 (2002).

855 35. Kuenze, G. *et al.* Allosteric mechanism for KCNE1 modulation of KCNQ1 potassium channel

856 activation. *Elife* **9**, (2020).

857 36. Li, P. *et al.* Differential modulations of KCNQ1 by auxiliary proteins KCNE1 and KCNE2. *Sci. Rep.* **4**,

858 4973 (2014).

859 37. Anderson, C. L. *et al.* Large-scale mutational analysis of Kv11.1 reveals molecular insights into type

860 2 long QT syndrome. *Nat. Commun.* **5**, 5535 (2014).

861 38. Nishio, Y. *et al.* D85N, a KCNE1 polymorphism, is a disease-causing gene variant in long QT

862 syndrome. *J. Am. Coll. Cardiol.* **54**, 812–819 (2009).

863 39. Kääb, S. *et al.* A large candidate gene survey identifies the KCNE1 D85N polymorphism as a possible

864 modulator of drug-induced torsades de pointes. *Circ. Cardiovasc. Genet.* **5**, 91–99 (2012).

865 40. Adler, A. *et al.* An International, Multicentered, Evidence-Based Reappraisal of Genes Reported to

866 Cause Congenital Long QT Syndrome. *Circulation* **141**, 418–428 (2020).

867 41. Glazer, A. M. *et al.* Arrhythmia Variant Associations and Reclassifications in the eMERGE-III

868 Sequencing Study. *Circulation* (2021) doi:10.1161/CIRCULATIONAHA.121.055562.

869 42. Choi, S. H. *et al.* Rare Coding Variants Associated With Electrocardiographic Intervals Identify

870 Monogenic Arrhythmia Susceptibility Genes: A Multi-Ancestry Analysis. *Circ Genom Precis Med* **14**,

871 e003300 (2021).

872 43. Van Driest, S. L. *et al.* Association of Arrhythmia-Related Genetic Variants With Phenotypes

873 Documented in Electronic Medical Records. *JAMA* **315**, 47–57 (2016).

874 44. Coyote-Maestas, W., Nedrud, D., He, Y. & Schmidt, D. Determinants of trafficking, conduction, and

875   disease within a K+ channel revealed through multiparametric deep mutational scanning. *Elife* **11**,

876   (2022).

877   45.   Weile, J. *et al.* A framework for exhaustively mapping functional missense variants. *Mol. Syst. Biol.*

878   **13**, 957 (2017).

879   46.   Glazer, A. M. *et al.* Deep Mutational Scan of an SCN5A Voltage Sensor. *Circ Genom Precis Med* **13**,

880   e002786 (2020).

881   47.   Ng, C.-A. *et al.* A massively parallel assay accurately discriminates between functionally normal and

882   abnormal variants in a hotspot domain of KCNH2. *Am. J. Hum. Genet.* **109**, 1208–1216 (2022).

883   48.   Hoppe, U. C., Marbán, E. & Johns, D. C. Distinct gene-specific mechanisms of arrhythmia revealed

884   by cardiac gene transfer of two long QT disease genes, HERG and KCNE1. *Proc. Natl. Acad. Sci. U. S.*

885   *A.* **98**, 5335–5340 (2001).

886   49.   Nakajo, K., Ulbrich, M. H., Kubo, Y. & Isacoff, E. Y. Stoichiometry of the KCNQ1 - KCNE1 ion channel

887   complex. *Proc. Natl. Acad. Sci. U. S. A.* **107**, 18862–18867 (2010).

888   50.   McDonald, T. V. *et al.* A minK–HERG complex regulates the cardiac potassium current IKr. *Nature*

889   **388**, 289–292 (1997).

890   51.   Ávalos Prado, P. *et al.* KCNE1 is an auxiliary subunit of two distinct ion channel superfamilies. *Cell*

891   **184**, 534-544.e11 (2021).

892   52.   Du, C., El Harchi, A., Zhang, H. & Hancox, J. C. Modification by KCNE1 variants of the hERG

893   potassium channel response to premature stimulation and to pharmacological inhibition. *Physiol*

894   *Rep* **1**, e00175 (2013).

895   53.   Esposito, D. *et al.* MaveDB: an open-source platform to distribute and interpret data from

896   multiplexed assays of variant effect. *Genome Biol.* **20**, 223 (2019).

897   54.   Karczewski, K. J. *et al.* The mutational constraint spectrum quantified from variation in 141,456

898   humans. *Nature* **581**, 434–443 (2020).

899 55. Remillard, C. V. & Yuan, J. X.-J. Activation of K+ channels: an essential pathway in programmed cell

900   death. *Am. J. Physiol. Lung Cell. Mol. Physiol.* **286**, L49-67 (2004).

901 56. Kowarz, E., Löscher, D. & Marschalek, R. Optimized Sleeping Beauty transposons rapidly generate

902   stable transgenic cell lines. *Biotechnol. J.* **10**, 647–653 (2015).

903 57. Mátés, L. *et al.* Molecular evolution of a novel hyperactive Sleeping Beauty transposase enables

904   robust stable gene transfer in vertebrates. *Nat. Genet.* **41**, 753–761 (2009).

905 58. Hermann, M. *et al.* Binary recombinase systems for high-resolution conditional mutagenesis.

906   *Nucleic Acids Res.* **42**, 3894–3907 (2014).

907 59. Thomas, G. P., Gerlach, U. & Antzelevitch, C. HMR 1556, a potent and selective blocker of slowly

908   activating delayed rectifier potassium current. *J. Cardiovasc. Pharmacol.* **41**, 140–147 (2003).

A (top) Schematic of KCNQ1 with HA-tag and KCNE1, CALM. (bottom) Structural surface model.

B Donut chart legend:
- Benign
- Likely Benign
- Likely Pathogenic
- Pathogenic
- VUS
- Conflicting
- Not Provided

C Venn diagram: Literature 49; ClinVar 106; gnomAD 101; overlaps 10, 7, 0, 32, 39, 37, 30; All Possible Missense 2451.

D WT-KCNE1 and KCNE1-HA current traces, I_{Ks} (pA/pF) vs Time (ms) and Test Potential (mV). Inset: 5s, −80mV to −40mV.

E KCNE1-HA and KCNQ1+KCNE1-HA imaging: dsRed, Alexa Fluor 647, Alexa Fluor 488, Merged Hoechst. Scale bar 5μm.

F KCNE1 variants D76N, L51H, WT (+KCNQ1); WT, Empty (−KCNQ1) vs Alexa Fluor 647 (Anti-HA).

Trafficking
0   1   2
Function

KCNE1   KCNQ1   CALM

A   g   g

B

C

D

E   F   G

F   V241   D242   F127   Y65   M62   Q260   F123   S68

G   F78   I82   Y81   W87